Observations of Seasonal Variation in the Ekman Layer

REBECCA R. SCHUDLICH

School of Oceanography, University of Washington, Seattle, Washington

JAMES F. PRICE

Woods Hole Oceanographic Institution, Woods Hole, Massachusetts

(Manuscript received 17 February 1994, in final form 20 September 1996)

ABSTRACT

The seasonal variation in the Ekman layer is examined using observations from the Long-Term Upper Ocean Study (LOTUS), including surface meteorology, current, and temperature. The near-surface current is found to be coherent with the wind at low frequencies (periods greater than one day). Using a wind-relative averaging method, the authors find the observed near-surface volume transport to be consistent with Ekman transport. The mean current profile has a spiral shape that is flat compared to the classic Ekman spiral in that it rotates less with depth than does the Ekman spiral. The mean current *e*-folds over 12 m in the summer and 25 m in the winter, with a decay in amplitude that implies eddy viscosities of 60×10^{-4} and 250×10^{-4} m^2 s^{-1}, respectively. Diurnal cycling is the dominant mode of variability in the summer and it determines the vertical structure of the spiral. In the winter, diurnal cycling is almost nonexistent due to greatly reduced solar insolation and stronger winds. A persistent downwind shear exists in the upper 15 m during the winter, which is comparable in magnitude to both a logarithmic ''wall-layer'' shear and a bias induced by surface wave motion. Given the winter dataset alone, it would be hard to exclude either of these possibilities. However, the nearly complete absence of this downwind shear in summer (fair weather) conditions is more consistent with the source being a wave-induced bias, or possibly Langmuir circulations.

1. Introduction

Ekman (1905) developed a theory for wind-driven flow in the surface layer of the ocean by assuming a balance between wind stress and the Coriolis acceleration. According to this theory the wind-driven flow in the upper ocean satisfies the vertically integrated Ekman balance

$$\int_0^{z_r} (u, v)\, dz = (\tau_y, -\tau_x)/\rho f, \qquad (1)$$

where z_r is the depth over which wind stress (τ_x, τ_y) is distributed in the upper ocean, (u, v) is the wind-driven current, and f is the Coriolis parameter. Ekman originally solved the corresponding differential equation assuming a constant viscosity. The resulting current profile spirals clockwise with depth (in the Northern Hemisphere), and the surface current $V_0 = \tau/\rho(Af)^{1/2}$ is 45° to the right of the wind. For a given constant vertical viscosity A, the depth scale of the Ekman current spiral is $D = (2A/f)^{1/2}$, and A is then the only unknown in this relation.

Many attempts have been made to verify Ekman's theory with observations. Several studies have shown that upper-ocean currents have a spiral structure, but generally with systematic differences from the spiral given by a constant viscosity. Richman et al. (1987) found a general clockwise turning of the current with depth, though with a large component of shear in the downwind direction near the surface that showed no turning. Clockwise turning mean current spirals that decay smoothly with depth have been observed by numerous investigators (Weller 1981; Davis et al. 1981; Price et al. 1986; Price et al. 1987; Weller et al. 1991; Rudnick and Weller 1993; Wijffels et al. 1994; Chereskin 1995; Weller and Plueddemann 1996; Lee and Eriksen 1996). Several of them observe a spiral whose rotation with depth is much ''flatter'' than an Ekman spiral in that the observed current rotates less with depth than predicted by Ekman's theory. Spurred by such observations, there have been many modifications of the basic theory, particularly in the specification of the vertical viscosity. Kraus (1993) presents a tensor analysis of Ekman flow, and Huang (1979) reviews ''turbulent'' Ekman theories that allow the eddy viscosity to vary with time and depth. These theories result in current

Corresponding author address: Dr. Rebecca R. Schudlich, School of Oceanography, University of Washington, Box 357940, Seattle, WA 98195-7940.
E-mail: rebecca@ocean.washington.edu

spirals with a somewhat different vertical structure, but there is no clear consensus on how the eddy viscosity depends on depth (Huang 1979). Estimates of the wind-driven transport in the past often differed from the Ekman transport by as much as a factor of 2 (Price et al. 1986; Richman et al. 1987).

Many attempts to isolate Ekman flow in the ocean have been hampered by the lack of datasets that sample the upper ocean with vertical resolution sufficient to capture the vertical structure of the Ekman current, and over a duration sufficient to resolve wind-driven flow relative to much larger pressure-driven flows. The local wind-driven flow is likely to be obscured by energetic mesoscale eddies and internal waves. The traditional approach in analyzing upper-ocean currents has been to subtract a deep ''reference'' velocity in order to isolate the local wind-driven flow (Davis et al. 1981; Price et al. 1987; Weller et al. 1991). Price et al. (1987) introduced a wind-coherent ensemble average approach that greatly improved success in isolating the Ekman signal. More recently, Chereskin and Roemmich (1991) developed a method using simultaneous hydrographic and acoustic Doppler measurements in which direct calculations of the geostrophic current were subtracted from the total measured current to yield an estimate of the wind-driven current. This approach has led to improved agreement between Ekman transport and observations, if not the classic Ekman profile, even in relatively short data records (Wijffels et al. 1994). Lee and Eriksen (1996) use a different method to estimate geostrophic currents, calculating the horizontal pressure gradient from density measured with a horizontal array of instruments in the upper ocean. This also resulted in improved agreement with Ekman transport.

In this paper we present observations from the Long Term Upper Ocean Study (LOTUS), expanding on results reported previously by Price et al. (1987) by including discussions of the robustness of the mean current, details of the diurnal cycle, estimates of horizontal stress divergence, and analysis of data from a later portion of LOTUS. We describe the field experiment in section 2. In section 3, we review a wind-relative averaging method used to form long-term means. Because stratification has a strong seasonal variation at the LOTUS site in the western Sargasso Sea, we separate our analysis into two periods: the summer (LOTUS 3) period and the winter (LOTUS 4) period. In section 4, we discuss the mean upper-ocean current during these two portions of the LOTUS experiment, and in sections 5 and 6 we discuss the dominant features of the mean current in each season. In section 7 we conclude with a summary and remarks on remaining issues.

2. Overview of the LOTUS experiment

a. The field program

The Long Term Upper Ocean Study was designed to provide continuous measurements of upper-ocean variability with high vertical resolution and at 15-min intervals over a period of two years (Briscoe and Weller 1984). The first LOTUS moorings were set in May 1982 at Site L (34°N, 70°W), well south of the mean axis of the Gulf Stream, and far from any significant bottom topography. A surface-moored 3.5-m discus buoy provided a platform for meteorological measurements as well as current and temperature measurements in the upper 300 m (Fig. 1). Surface mooring 767 (designated LOTUS 3; LOTUS 1 and 2 were earlier tests) was replaced by 770 (LOTUS 4) in October 1982, and the entire array was replaced in April 1983 (LOTUS 5 and 6).

Meteorological measurements were made with a vector averaging wind recorder on the surface buoy. Currents and temperature in the upper 100 m were measured primarily with vector-measuring current meters (VMCMs), which are designed to resolve relatively weak mean upper-ocean currents in the presence of the large and rapidly oscillating orbital velocities associated with surface waves (Weller and Davis 1980). Below 100 m, as well as at some shallower depths, currents were measured primarily with vector-averaging current meters (VACMs) (Fig. 1).

b. Oceanic conditions during LOTUS

During the course of the LOTUS experiment, stratification in the upper ocean varied on diurnal and seasonal timescales, as well as those associated with passing eddies (Briscoe and Weller 1984). The LOTUS 3 period spanned 170 days, 14 May to 31 October 1982. Meteorological conditions were dominated by fair summer weather typical of the subtropics. Strong solar heating together with light winds caused the formation of diurnal stratification during the daytime, which had surface amplitudes of 0.3° to 2.0°C in the summer (Stramma et al. 1986). The seasonal cycle of the net heat flux created a strong seasonal thermocline, and the surface temperature warmed by about 10°C over the summer (Bowers et al. 1986). The seasonal thermocline began to erode at the end of LOTUS 3 and continued to erode throughout the LOTUS 4 period, which spanned 109 days (31 October 1982 to 19 February 1983). LOTUS 4 was dominated by winter weather conditions, with even more cloudiness than typical for the region (Deser et al. 1983). Net cooling at the ocean surface and strong winds combined to suppress the diurnal cycle and cause the convection that forms the 18° Water in the North Atlantic (Worthington 1959).

The currents measured at the LOTUS site show energetic, vertically coherent events (Fig. 2) that sometimes extended as deep as 4000 m. Some of these events were Gulf Stream rings, and some appeared to be anticyclonic eddies (Briscoe and Weller 1984). The rms speed of these low-frequency motions was 25 cm s^{-1} (Briscoe and Weller 1984), about five times as large as the O(5 cm s^{-1}) wind-driven surface currents of interest

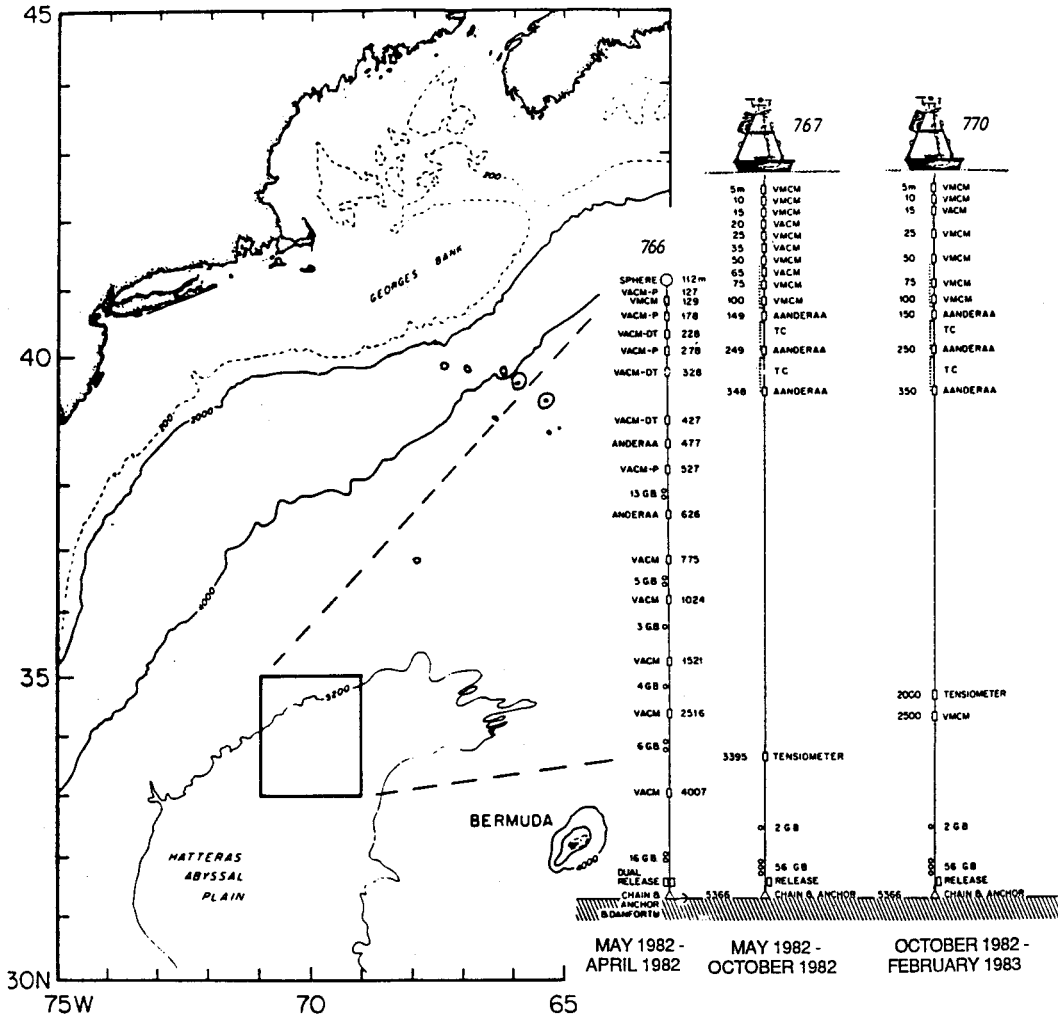

FIG. 1. The location of the Long Term Upper Ocean Study area and diagrams of three LOTUS moorings at sea for the first year of the experiment (from Tarbell et al. 1984). Surface mooring 767 was at sea for the LOTUS 3 period and was replaced by surface mooring 770 for the LOTUS 4 period. The subsurface mooring 766, used for data below 100 m for the LOTUS 4 period, was positioned 7.9 km NNW of the surface mooring. The total water depth at the site is approximately 5300 m.

here. These non-wind-driven currents present a major signal-to-noise problem for our analysis. For example, coherence between the total upper-ocean current and the wind is nearly zero at all frequencies.

3. A wind-relative averaging method

In our analysis of the wind-driven current, we perform a series of steps to overcome the signal-to-noise ratio problem and extract the wind-driven current from the total measured current. The method is based on the traditional approach of referencing currents to a depth below the mixed layer, but then further enhances the wind-driven signal by rotating the current into a coordinate system aligned with the local wind averaged over 1-day subintervals. This essentially amounts to forming a wind-relative average of the current over a given frequency range. The long-term wind-relative mean is formed from an ensemble average of the individual wind-relative means. This is the ''coherent ensemble average'' method introduced by Price et al. (1987), where it is described briefly. This approach has since been shown to enhance the Ekman signal in many datasets (Weller et al. 1991; Wijffels et al. 1994, Gnanadesikan 1994; Lee and Eriksen 1995; Weller and Plueddemann 1996).

The first step in this analysis is to isolate the wind-driven flow from the flow driven by the pressure gradient by subtracting a deep current from the upper-ocean current. This approach necessarily assumes that the pressure-driven flows are vertically uniform above the reference depth. The eddy motions that dominate the total current during the LOTUS experiment were fairly barotropic, that is, vertically uniform, in the upper 500 m

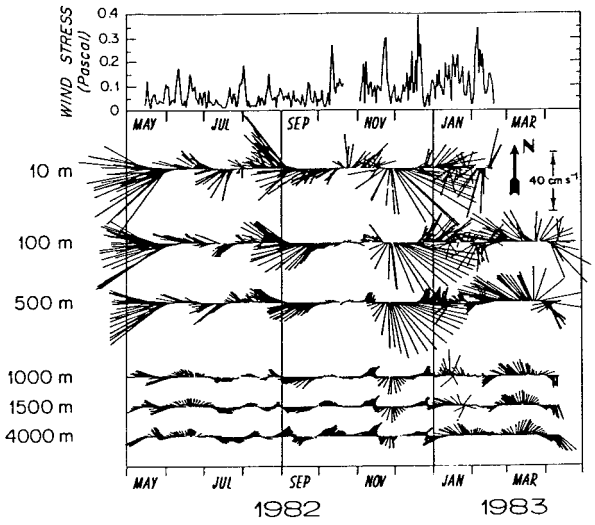

FIG. 2. Wind stress and current time series from the first year of the LOTUS experiment (from Briscoe and Weller 1984). Each current vector is an average over one day. Energetic mesoscale motions dominated the observed currents and were often coherent through the entire water column.

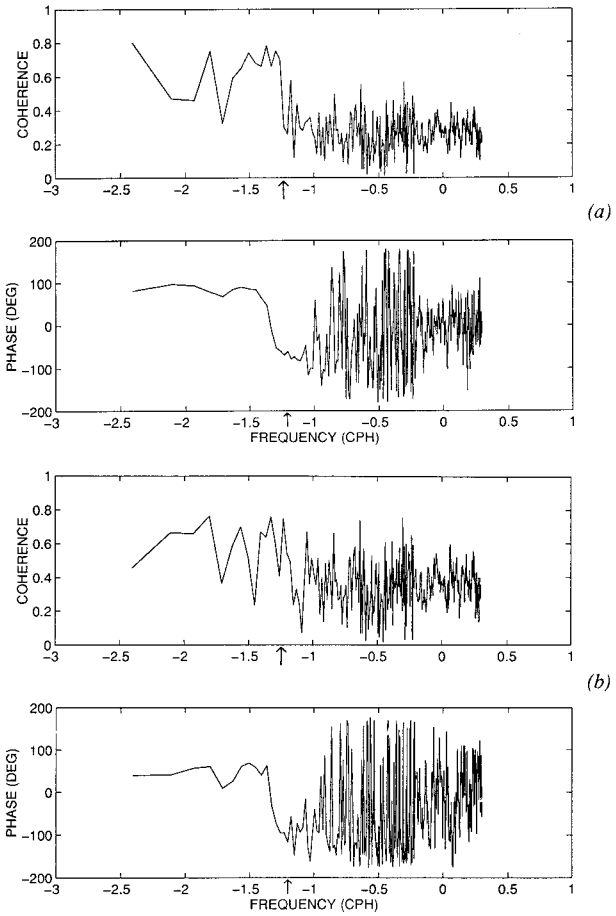

FIG. 3. (a) Coherence and phase (in degrees) of the clockwise cross-spectrum between wind stress and 10-m current observed during the LOTUS 3 period. The current at 50 m has been subtracted from the 10-m current; the choice of a reference level is discussed in the text. (b) Coherence and phase (in degrees) of the clockwise cross-spectrum between wind stress and 10-m current observed during the LOTUS 4 period. In this case the current at 129 m has been subtracted from the 10-m current; the choice of a reference level is discussed in the text. The arrows indicate the diurnal-inertial frequency (they are nearly identical at this latitude, 34°N).

(Fig. 2). Most of the baroclinic structure of the eddy motions was in the main thermocline between 500 and 1000 m (Lippert and Briscoe 1990). Thus, by referencing the LOTUS upper-ocean currents to a depth of O(100 m) much of the eddy ''noise'' can be removed. In fact, at low frequencies (greater than an inertial period), the currents at 10 m relative to a deeper reference current are found to be highly coherent with the wind direction (Fig. 3). At frequencies below about 0.02 cph, the current at 10 m is approximately 90° to the right of the wind, consistent with an Ekman balance.

Since even the very small amounts of stratification associated with diurnal warming can limit the penetration of wind stress into the water column (Price et al. 1986), the reference level should be chosen to be deeper than the mixed layer depth. However, the deeper the reference level, the greater the likelihood that geostrophic shear or internal wave motions will contaminate the wind-driven current. Since geostrophic currents cannot be estimated directly with the LOTUS observations, our goal was to choose a reference level deeper than the mixed layer, but not excessively so. In practice, the choice of z_r is dictated in part by data availability, and later in this paper we show the consequences of choosing several different reference depths. The analysis presented in Fig. 3 is not particularly sensitive to the choice of the reference level; however, estimates of transport will be somewhat sensitive to reference depth, as discussed further in section 4c.

Price et al. (1987) introduced the idea of analyzing currents in a natural coordinate system aligned with the wind. To rotate the currents into a wind-relative coordinate system, wind stress and ocean current records are first vector-averaged over subintervals of one day (the sensitivity to this subinterval length is checked in section 4c), and then each daily average was rotated into a crosswind, downwind coordinate system wherein the wind stress vector points along the positive y axis such that (τ_x, τ_y), as utilized in (1), are equal to $(0, |\boldsymbol{\tau}|)$.

Finally, the individual, wind-relative daily averages of the current are ensemble-averaged to form the mean over a season. In effect, this coordinate system follows the low-frequency variations in the wind direction and therefore helps to isolate the wind-driven current. By analyzing the data this way, the average wind stress is increased by about a factor of 4, to 0.068 Pa during LOTUS 3 (when the simple time-mean wind stress is 0.015 Pa), and to 0.147 Pa during LOTUS 4 (when the simple time mean is 0.040 Pa). The final mean current is then interpreted as if the wind had blown in a constant direction during the observation period.

An alternate way to describe this wind-relative averaging method was presented by Weller et al. (1991). As they note, their method is equivalent to performing a regression between the current and a unit vector pointing in the direction of the wind [see Gnanadesikan (1994) for additional explanation of the wind-coherent method and its application to data from the MILDEX and SWAPP experiments]. The 24-h boxcar average we use is equivalent to a 48-h low-pass filter and thus eliminates both diurnal and inertial motions at the latitude of the LOTUS observations. The wind-relative average we describe here is therefore simply an alternative way to examine the low-frequency Ekman-like current structure shown in the cross spectra of Fig. 3.

a. Data dropouts and averaging intervals

During the LOTUS 3 period the vector-averaging wind recorder failed on 21 October 1982, 160 days after its deployment. Since nearly all of our calculations are tied to wind measurements, we truncated all other records to 160 days also. Eleven days later, the surface mooring was replaced, and the LOTUS 4 deployment began. Also during LOTUS 3, the VMCM at 5-m depth failed after 86 days. After determining that the mean meteorological fluxes over the first 86 days were almost identical to the means over the full 160 days, and that numerical simulations gave nearly identical results over these two periods (Price et al. 1987), we chose not to truncate the other records to this length. The mean current at 5-m depth for LOTUS 3 is thus an 86-day average. The VMCM at 15-m depth was fouled by a garbage bag, apparently dumped from a passing ship, which caught in the rotor of the VMCM midway through LOTUS 3 (Tarbell et al. 1984). It came free of the instrument after 11 days without damaging the rotor and the VMCM functioned normally after that. We therefore excluded the 11 ''garbage bag'' days of current measurements at 15 m from our calculations but otherwise treated the 15-m data normally. The mean 15-m current is thus a 149-day average. At 10 and 25 m, mean currents are 160-day averages.

During the LOTUS 4 period currents and temperature were measured from a surface mooring at depths of 5, 10, 25, 50, 75, and 100 m by VMCMs and at 15 m by a vector-averaging current meter. Currents at 129 m and deeper were measured from a subsurface mooring (Fig. 1). The 25-m VMCM failed after 99 days, and the 75-m VMCM failed after 50 days. We treated these records in the same way as the failed 5-m VMCM in LOTUS 3 (i.e., the average current at 25 m is a 99-day mean, and the average current at 75 m is a 50-day mean). The VMCM at 100-m depth failed after only 8 days. Because the extreme shortness of this record results in a statistically insignificant mean, we exclude the 100-m current from our calculations. At all other depths (5, 10, 25, and 129 m) the mean currents during LOTUS 4 are 109-day averages.

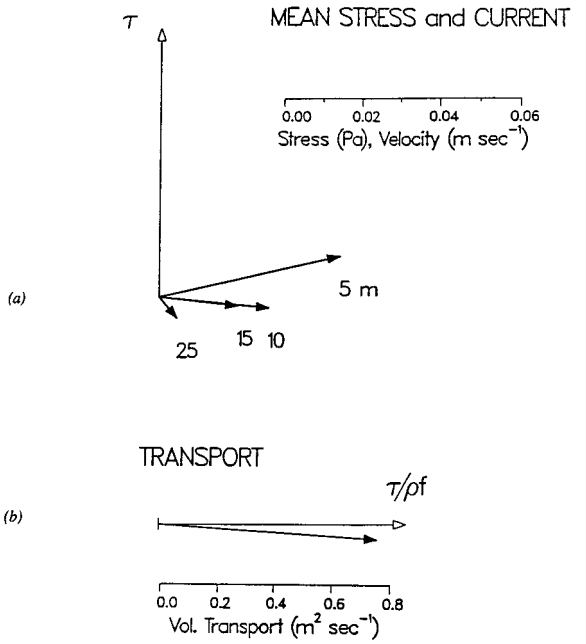

FIG. 4. (a) Wind-relative mean wind stress, current spiral, and (b) transport relative to 50 m from the LOTUS 3 observations. The wind stress vector is arbitrarily pointed up, or ''north,'' and is shown with an open arrowhead; current vectors are shown with solid arrowheads. Numbers at the ends of the current vectors indicate the depth in meters. The theoretical Ekman volume transport equal to $\tau/\rho f$ is shown with an open arrowhead, and the observed transport relative to 50 m is shown with a solid arrowhead. Uncertainties are given in Tables 1 and 2. (Adapted from Price et al. 1987.)

4. Mean spiral and transport

a. LOTUS 3—summer

The mean current at the four VMCM depths above 50 m and the resulting transport for LOTUS 3 (summer) are shown in Fig. 4. Numerical values for the mean velocity at each depth and their uncertainties (standard errors) are listed in Table 1. The mean currents at 15 m and above are well defined, and the 25-m value is not distinguishable from zero.

As described by Price et al. (1987), the mean current spiral is strongly surface trapped during LOTUS 3. The current decays rapidly with depth, *e*-folding over about a 12-m scale. The current at 5 m has an amplitude of about 4 cm s^{-1} and is about 78° to the right of the wind. The current rotates clockwise only about 20° over the *e*-folding depth and thus is ''flat'' compared to the classic Ekman spiral, which predicts a rotation of about 60° over an *e*-folding depth for a constant eddy viscosity. Relatively flat spirals have also been detected in other observations of the mean wind-driven current (Weller 1981; Price et al. 1986; Wijffels et al. 1994; Chereskin 1995). This mismatch between the amplitude decay and rotation of the mean current spiral can be expressed in terms of the eddy viscosity, estimated to be 60×10^{-4} m^2 s^{-1} based on the *e*-folding of the current's amplitude and 540×10^{-4} m^2 s^{-1} based on the current's rotation

TABLE 1. Mean current and uncertainties during the LOTUS 3 and 4 periods. Uncertainties on the data are statistical standard errors; 90% confidence limits are larger by a factor of 1.7, and 95% confidence limits are larger by a factor of 2.0. Calculating the standard error requires an estimate of the integral timescale, estimated from the data using a standard statistical definition (Bevington 1969). The integral timescale for the daily values was 1.5 days, so the number of effective degrees of freedom used to estimate the standard error for the 160-day record was taken to be $160/(2 \times 1.5) = 53$.

	LOTUS 3 (summer)		LOTUS 4 (winter)	
Depth (m)	Crosswind current (cm s^{-1})	Downwind current (cm s^{-1})	Crosswind current (cm s^{-1})	Downwind current (cm s^{-1})
5	4.6 ± 1.2	1.0 ± 0.7	5.0 ± 1.8	5.4 ± 1.5
10	2.8 ± 0.7	−0.3 ± 0.4	4.7 ± 1.7	3.5 ± 1.5
15	2.0 ± 0.7	−0.2 ± 0.5	4.3 ± 1.8	0.2 ± 1.5
25	0.4 ± 0.4	−0.5 ± 0.4	2.6 ± 1.5	0.5 ± 1.3
50*	—	—	2.1 ± 1.5	−0.1 ± 1.4
75	0.6 ± 0.3	−0.2 ± 0.4	0.7 ± 1.2	−0.3 ± 1.0
100	1.1 ± 0.6	−0.7 ± 0.6	−1.4 ± 1.3	−0.5 ± 0.8
129**			—	—

* The 50-m depth was used as the reference level for the LOTUS 3 period. The simple time-mean current at this depth was 18.1 cm s^{-1} westward and 0.7 cm s^{-1} northward.

** The 129-m depth was used as the reference level for the LOTUS 4 period; the simple time-mean current at 129 m was 1.8 cm s^{-1} westward and 4.4 cm s^{-1} northward.

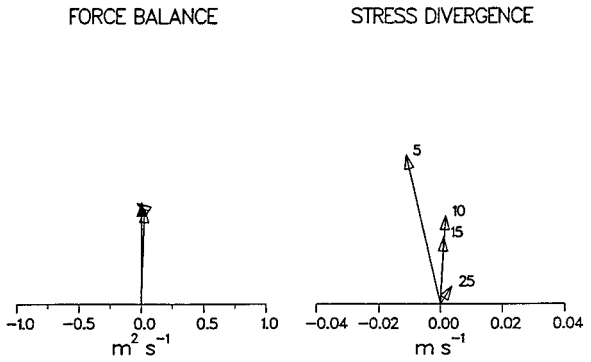

FIG. 5. Mean force balance and horizontal stress divergence ($\partial\tau/\partial z$) during LOTUS 3. The mean wind direction is ''up'' as in Fig. 4. The estimated mean profile of $\partial\tau/\partial z$, calculated from the observed current as described in the text, is shown on the right. Numbers at the tips of the vectors indicate the depth in meters. The mean wind stress vector is shown on the left with a solid arrowhead. The Coriolis force vector has an open arrowhead and is plotted with the same origin as the wind stress; the acceleration vector is also shown with an open arrowhead but is plotted with its tail at the tip of the Coriolis vector. The small net acceleration reflects the close agreement with the Ekman balance in the LOTUS 3 observations. The nearly exact force balance confirms that the estimated $\partial\tau/\partial z$ is robust.

(Price et al. 1987). For summer conditions in the Pacific with winds slightly stronger than those of LOTUS 3, Chereskin (1995) estimated slightly larger values: an *e*-folding scale of 25 m and an eddy viscosity of 274 and 1011×10^{-4} m^2 s^{-1} for amplitude decay or rotation rate, respectively.

Estimates of volume transport are obtained by integrating the mean current profile using a simple trapezoidal method. For the LOTUS 3 period, the estimated volume transport between 50 m and the surface agrees quite well with the theoretical Ekman transport (within about 10%) both in magnitude and direction (Fig. 4b; Table 2). This is well within the likely error of the wind stress, about 20% as estimated using the bulk aerodynamic method of Large and Pond (1981).

The good agreement with the simple Ekman momentum balance suggests that it should be possible to calculate meaningful estimates of horizontal stress divergence ($\partial\tau/\partial z$) in the upper ocean. Based on the local momentum balance

$$\frac{\partial v}{\partial t} + fu = \frac{1}{\rho}\frac{\partial \tau_y}{\partial z} \tag{2}$$

the horizontal stress divergence can be estimated from the observed mean current and acceleration. The acceleration term is calculated as the net change in velocity at each VMCM depth over each daily average, then rotated relative to wind direction and averaged over the entire record. The Coriolis term is calculated simply as the observed mean current at each depth multiplied by the Coriolis frequency. The accuracy of this estimate of $\partial\tau/\partial z$ can be independently checked by integrating the terms on the left-hand side of (2) and comparing their vector sum to the observed surface wind stress τ. This comparison is essentially a check of the force balance between the Coriolis force, wind stress, and local acceleration. If the balance is exact, then the vector sum of the acceleration and the Coriolis force should equal the wind stress.

The results of this calculation reveal a mean $\partial\tau/\partial z$ that decays monotonically with depth (Fig. 5). There is significant wind stress penetration to about 15 m. The

TABLE 2. Mean transport and errors. The Ekman transport was computed using mean wind stress magnitudes of 0.068 and 0.147 Pa (LOTUS 3 and 4, respectively), which are presumed to be uncertain to 20% because of uncertainty inherent in the bulk aerodynamic method (Large and Pond 1981). The standard error for the Ekman transport estimate (based on 109 daily estimates over the LOTUS 4 record) is ±0.21 m^2 s^{-1}.

	LOTUS 3 (summer)		LOTUS 4 (winter)	
	Crosswind transport (m^2 s^{-1})	Downwind transport (m^2 s^{-1})	Crosswind transport (m^2 s^{-1})	Downwind transport (m^2 s^{-1})
Observed	0.72 ± 0.19	−0.05 ± 0.14	1.71 ± 1.21	0.65 ± 1.03
Ekman	0.82 ± 20%	(0)	1.76 ± 20%	(0)

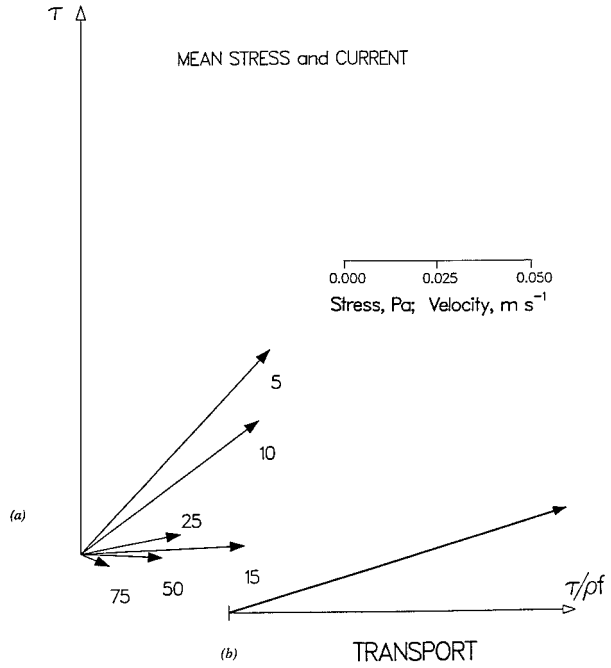

FIG. 6. (a) Mean current spiral and (b) transport during the LOTUS 4 period. Uncertainties are given in Tables 1 and 2. The wind stress vector is arbitrarily pointed up, or ''north,'' and is shown with an open arrowhead; current vectors are shown with solid arrowheads. Numbers at the ends of the current vectors indicate the depth in meters. The theoretical Ekman volume transport equal to $\tau/\rho f$ is shown with an open arrowhead, and the observed transport relative to 129 m is shown with a solid arrowhead. Uncertainties are given in Tables 1 and 2. As described in the text, the 75-m current is a 50-day average, the 25-m current is a 99-day average, and all other currents are 109-day averages. Note that the current spiral has a large downwind shear in the upper 15 m, and the shear abruptly changes to the crosswind direction below 15 m. The observed transport agrees with the predicted Ekman transport except for the large downwind component.

vertical structure of $\partial\tau/\partial z$ mirrors the structure of the mean current (see Fig. 4), reflecting that the mean current is in Ekman balance, as does the very small net acceleration.

b. LOTUS 4—winter

The mean current profile for LOTUS 4 is found by referencing currents to 129 m and averaging relative to the wind direction as described in section 3. Mean wind stress during LOTUS 4 was 0.147 Pa, more than twice the LOTUS 3 mean. The mean currents above the reference level at 129 m and the resulting transport are shown in Fig. 6 (notice that this figure is plotted on a different scale than is Fig. 4). The mean currents at 50 m and above are well defined, but the mean currents at 75 and 100 m are not distinguishable from zero. Numerical values for the mean velocity at each depth and their uncertainties (as standard errors) are listed in Table 1.

The LOTUS 4 mean wind-driven current profile is somewhat different from the LOTUS 3 spiral, being spread over a greater vertical scale, in some ways appearing more like a classic Ekman spiral. The current at 5 m has an amplitude of about 7 cm s^{-1} and is about 43° to the right of the wind. The mean current decays with an *e*-folding scale of about 25 m and rotates clockwise about 36° over the *e*-folding depth. The resulting eddy viscosities are 250×10^{-4} m^2 s^{-1} for shear and 650×10^{-4} m^2 s^{-1} for rotation, the former being substantially larger than that inferred from the LOTUS 3 mean spiral for summer conditions, but similar to the 5-month (January to June) average value of 360 ($\pm$130) $\times 10^{-4}$ m^2 s^{-1} and *e*-folding scale of 33 m estimated from FASINEX data (Lee and Eriksen 1996).

The shear in the winter-mean current profile has a very different character than found in the summertime LOTUS 3 spiral. In the upper 15 m, the shear is almost entirely in the direction of the wind (downwind). Below 15 m, the shear is almost entirely perpendicular to the wind and thus looks qualitatively like the LOTUS 3 spiral (Fig. 4). The downwind shear in the upper 15 m is a puzzling feature of the winter observations since no such downwind shear was observed in the summer. Richman et al. (1987) also observed a strong downwind shear in the upper 9 m of the water column in the Pacific Ocean under conditions of moderately strong wind stress (0.145 Pa), as did Weller and Plueddemann (1996) under more moderate wind stress (0.049 Pa). We examine the near-surface downwind shear during LOTUS 4 in more detail in section 6.

While the winter current spiral may appear more Ekman-like than the summer spiral, its transport does not agree as well with the Ekman balance (Fig. 6), having a large downwind component (though due to the greatly increased uncertainty in the LOTUS 4 mean currents, the Ekman transport is well within one standard error of the observed transport). Nevertheless, without the downwind component of current, agreement with the theoretical Ekman transport would be the same as was found for the summer portion of the LOTUS observations. About half of the observed downwind transport results from the downwind shear in the upper 15 m of the mean current profile (see Table 2).

c. Sensitivity of the mean current and transport

1) SENSITIVITY TO REFERENCE LEVEL

How sensitive are our results to the reference level chosen? Our choice of reference level was based on estimates of mixed layer depth using a temperature difference of 0.05°C from the surface. Based on these estimates, we chose a reference depth of 50 m for LOTUS 3. This reference depth was below the mixed layer and within the seasonal thermocline for all but the last few days of the LOTUS 3 deployment (Price et al. 1987). Similar reference levels have been used for upper-ocean currents observed under relatively calm to moderate

TABLE 3. Sensitivity of observed transport calculation to reference level. The Ekman transport during LOTUS 3 and LOTUS 4, respectively, is 0.82 $m^2\ s^{-1}$ and 1.76 $m^2\ s^{-1}$.

Reference level (m)	LOTUS 3 (summer)		LOTUS 4 (winter)	
	Crosswind transport ($m^2\ s^{-1}$)	Downwind transport ($m^2\ s^{-1}$)	Crosswind transport ($m^2\ s^{-1}$)	Downwind transport ($m^2\ s^{-1}$)
15	0.30	0.08	0.07 ± 0.60	0.03 ± 0.06
25	0.59	0.19	0.41 ± 0.53	0.16 ± 0.15
50[a]	0.72	−0.05	0.62 ± 0.75	0.25 ± 0.19
75[b]	0.34	0.06	0.99 ± 0.48	0.76 ± 0.38
100[c]	−0.10	0.47	2.96 ± 1.62	0.84 ± 1.09
129[d]			1.71 ± 0.52	0.65 ± 1.03

[a] Based on estimated mixed layer depth and observed temperature stratification, the reference level used for the LOTUS 3 period was 50 m.

[b] During LOTUS 4, the VMCM at 75 m failed after 50 days. The mean wind stress during this period was 0.140 Pa and the predicted Ekman transport was 1.68 $m^2\ s^{-1}$.

[c] During LOTUS 4, the VMCM at 100 m failed after only 8 days. The mean wind stress during this period was 0.137 Pa and the predicted Ekman transport was 1.64 $m^2\ s^{-1}$.

[d] The reference level used for the LOTUS 4 period was 129 m. If the VMCM at 100 m had not failed, it would have been the reference level selected based on observed temperature stratification and estimated mixed layer depths.

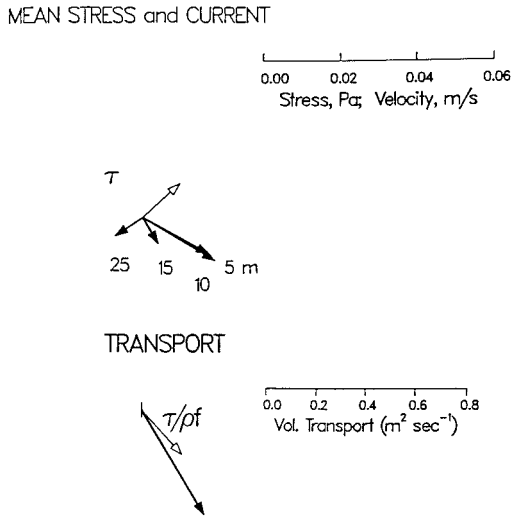

FIG. 7. Simple time mean of wind stress and currents from the LOTUS 3 period and the resulting transport relative to 50 m in a geographic east, north coordinate system. The wind stress and the theoretical Ekman transport are shown with open arrowheads; the observed currents and transport relative to 50 m are shown with solid arrowheads. Numbers at the ends of the current vectors indicate the depth in meters. Notice that the average wind stress is significantly reduced from the wind-relative averaging method and agreement with Ekman transport is poor (compare to the wind-relative mean, Fig. 4).

winds (Weller 1981; Chereskin 1995; Weller and Plueddemann 1996).

While the structure of the current spiral is relatively insensitive to the choice of reference level, the integrated volume transport does depend on the reference level. Fortunately the current meter spacing on the LOTUS 3 mooring was such that observations existed at at least one depth (50 m) that was appropriate for a reference level. Had we referenced the velocities to the current measured at 25 m (the next shallowest VMCM) the estimated transport is only about three-quarters of the Ekman transport (Table 3). Referencing currents to VMCMs deeper than 50 m also causes the estimated transport to depart significantly from the Ekman volume transport; the departure increases with increasing depth, suggesting an increasing contribution from non-wind-driven currents. In an experiment with meteorological conditions similar to LOTUS 3 but with finer vertical resolution of currents, Chereskin (1995) found that any reference level between 48 and 60 m worked equally well to isolate Ekman transport.

During LOTUS 4 the mixed layer depth was quite variable but was always shallower than 100 m (Schudlich 1991). In this sense, a reference level of 100 m would have been desirable and consistent with the criterion for choosing 50 m as the reference level for LOTUS 3. However, a reference level of 129 m seemed the only reasonable choice for the LOTUS 4 dataset since the VMCMs at 75 and 100 m failed early in the deployment. There were no other VMCMs on any of the LOTUS 4 moorings other than one at 2500 m (Fig. 1). On the adjacent subsurface mooring, current measurements deeper in the water column were made by a VACM at 178 m, which seemed excessively deep for a reference level based on our estimates of mixed layer depth during LOTUS 4. As in LOTUS 3, the estimated volume transport varies with the choice of a reference level. For example, if the currents are referenced to any of the current meters shallower than 100 m, the observed transport becomes a successively smaller fraction of the predicted Ekman transport (Table 3), suggesting that some of the wind-driven transport has been missed.

2) SENSITIVITY TO WIND-RELATIVE ROTATION

The use of a wind-relative coordinate frame is crucial to this analysis. For comparison, the mean current spiral and transport during LOTUS 3 when the simple time mean is taken *without* rotating into a wind relative frame is examined (Fig. 7). Agreement with Ekman transport is no better than in previous studies (Price et al. 1986; Richman et al. 1987), despite the greater length of the LOTUS dataset. The simple time average of wind stress is significantly less than the rotated average (0.015 Pa vs 0.068 Pa), as noted earlier. The wind-relative averaging method is especially apt for analyzing the LOTUS observations because the wind is quite variable, and this variability is at a higher frequency than the oceanic mesoscale variability. The wind-relative averaging method thus reduces the non-wind-driven part of the current without biasing the mean current, as it would in a region of steady winds and large mean currents (Wijffels et al. 1994; Lee and Eriksen 1996).

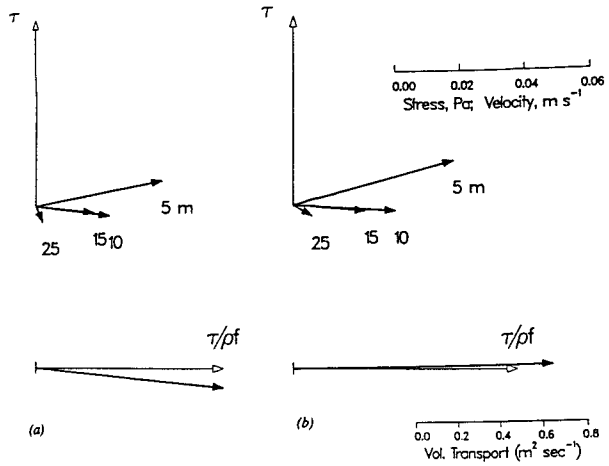

FIG. 8. Wind-relative mean spiral and transport for the LOTUS 3 period formed with individual averages over (a) 2 days and (b) 1 inertial period. The basic structure of the spiral and the volume transport are not significantly different from each other or from the mean formed with individual averages over one day (see Fig. 4).

3) SENSITIVITY TO AVERAGING SUBINTERVAL AND TOTAL RECORD LENGTH

The choice of a 1-day averaging subinterval for the wind-relative averaging method (§ 3) is somewhat arbitrary, but the resulting mean is not highly sensitive to this choice; similar ensemble averages formed with subintervals of either two days or one inertial period (21.5 h) are not significantly different (Fig. 8). As the length of the averaging subinterval is increased, the time mean of the currents and transport decrease until they reach a minimum when the averaging subinterval reaches its maximum value of the total record length (Fig. 7). This result is consistent with the stable phase relationship between the wind stress and the 10-m current (Fig. 3).

The mean current and transport are averages over long data records. This averaging is crucial to our analysis because, on any given day, the Ekman balance is not likely to be satisfied (Fig. 9). This imbalance is most likely true because the reference levels selected are optimum for the overall LOTUS 3 and LOTUS 4 records, but are too deep for some individual days so that some geostrophic shear is aliased into the daily estimates of transport. It is only by averaging over a sufficiently long time that an Ekman balance emerges (in other words, when using this method a large amount of averaging is required to reduce the non-Ekman terms in the equations of motion). Our calculations indicate that, during summer, the average crosswind component of observed transport begins to stabilize near the Ekman transport after about 60 days of averaging (Fig. 10). Similarly, the downwind component of observed transport begins to stabilize near zero after about 60 days and remains within a few percent of zero throughout the remainder of LOTUS 3. Variability in the daily transport estimates was greater during the winter LOTUS 4 period (Fig. 9). LOTUS 4 was also shorter than LOTUS 3 (109 vs 160 days). For both these reasons, the mean currents and transport for LOTUS 4 are thus less well defined in a statistical sense than for LOTUS 3 (see Tables 1 and

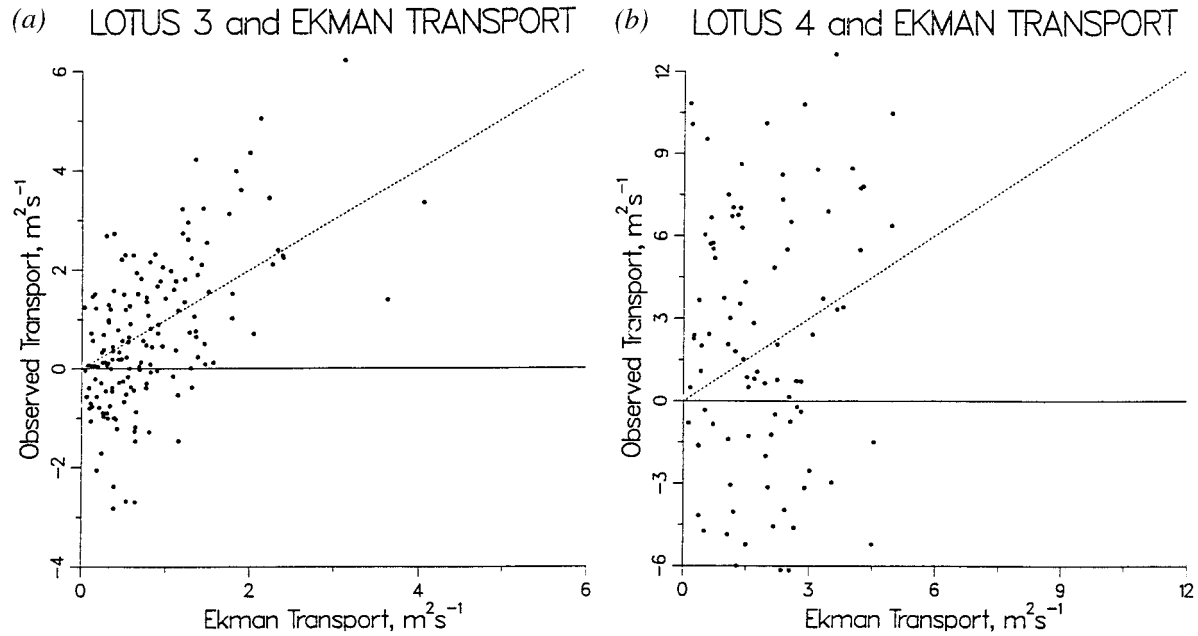

FIG. 9. (a) Daily estimates of the crosswind component of observed transport relative to 50 m for the LOTUS 3 period, plotted vs theoretical Ekman transport, and (b) daily estimates of crosswind observed transport relative to 129 m for the LOTUS 4 period plotted vs theoretical Ekman transport. Each point represents a daily average. The dashed line has a slope of one; if all days had exact agreement with Ekman transport, all the points would lie along this line.

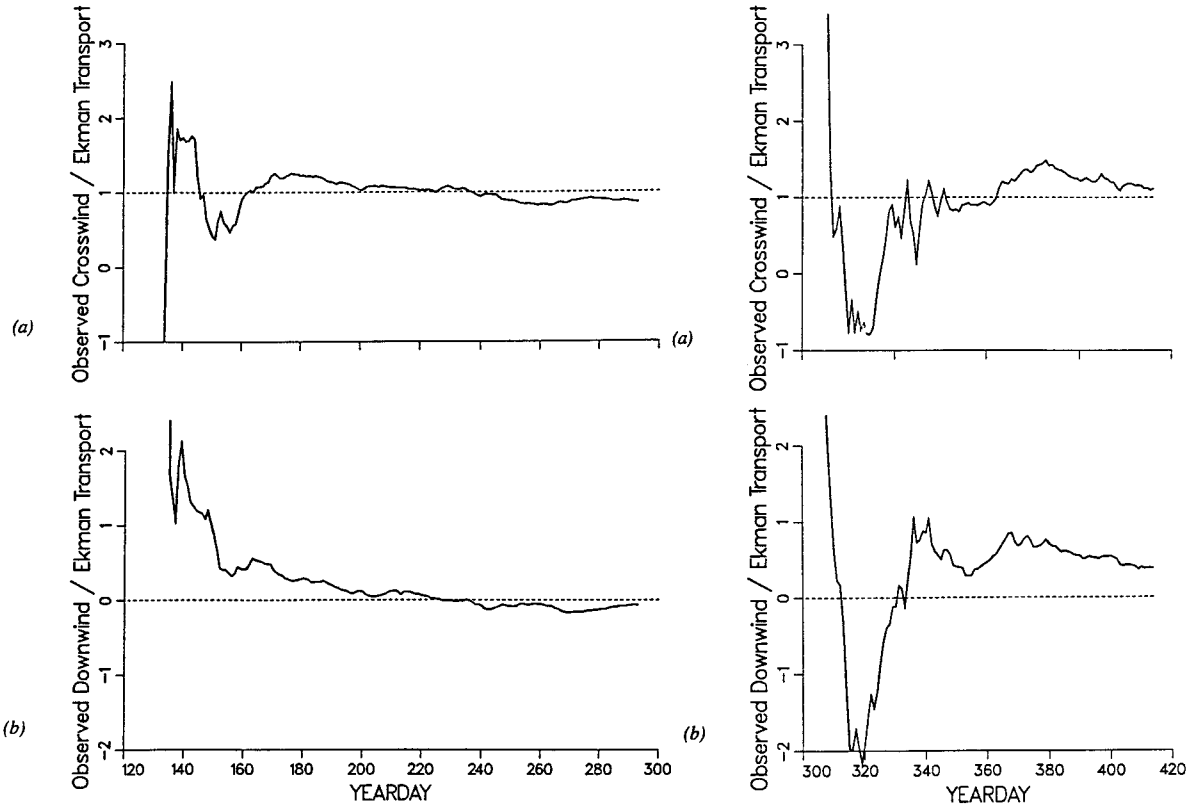

FIG. 10. Left column: (a) Cumulative average of crosswind component of observed transport during LOTUS 3 scaled by the Ekman transport. A ratio near 1 is attained after about 60 days. (b) Cumulative average of downwind component of observed transport scaled by the Ekman transport. A value near zero is attained after about 60 days. Right column: (a) Cumulative average of the ratio of observed crosswind transport to Ekman transport during the LOTUS 4 period. A ratio near 1 is attained only near the end of the 109-day record. (b) Cumulative average of the ratio of observed downwind transport to Ekman transport. Notice that the ratio remains positive (downwind) throughout the record.

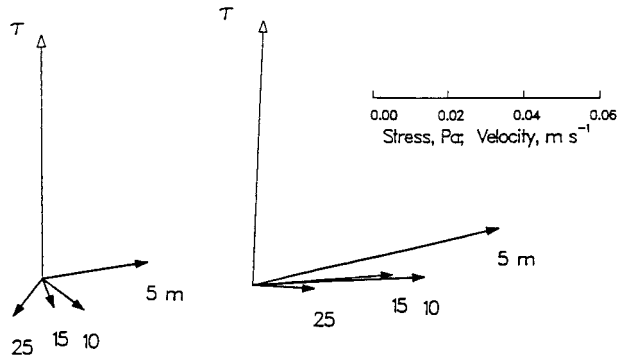

FIG. 11. Diurnal cycle of the LOTUS 3 mean wind stress and mean current spiral (relative to 50 m). The wind stress vector is shown with an open arrowhead, and the numbers at the end of the current vectors indicate the depth in meters. On the left is the mean current during nighttime hours (2000 to 0800 LST) of the LOTUS 3 data and on the right is the mean current during the daytime hours (0800 to 2000 LST). Note that there is little diurnal variation in the wind stress, while the diurnal variation in the current is considerable. (Adapted from Price et al. 1987.)

2). The average crosswind transport begins to approach the predicted Ekman transport only at the end of the 109-day record (Fig. 10). The downwind component of observed transport remains positive (in the same direction as the wind) throughout the final 80 days of the record. We discuss the downwind current further in section 6.

5. Diurnal variability of current spiral and transport

As Price et al. (1987) discuss, there is a large diurnal variability in the wind-driven current during LOTUS 3 that can be seen by forming separate ensemble averages over the daytime, 0800 to 2000 Local Solar Time (LST), and nighttime, 2000 to 0800 LST. The amplitude of the surface current is greatly increased in the daytime, when increased current shear can be supported by the stable stratification of the diurnal thermal cycle (Fig. 11). The shear is much reduced at night when cooling allows wind mixing to deepen the mixed layer well below its midday value.

The complete diurnal cycle of the mean LOTUS 3

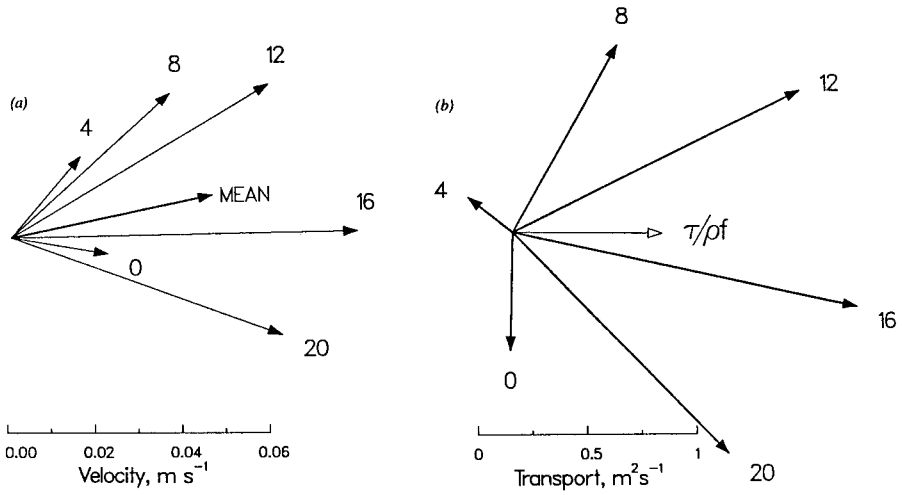

FIG. 12. Diurnal cycle of (a) the observed 5-m current (the heavy vector in the middle is the mean value) and (b) the observed transport (the light vector in the middle is the mean Ekman transport) during LOTUS 3. Both the current and transport are relative to 50 m. Numbers at the end of the vectors indicate the hour of day, LST. The 5-m current is greatest in midafternoon when the mixed layer is shallowest and smallest at night when the mixed layer is deepest. The diurnal cycle of transport reflects the strong diurnal cycle of the currents in the upper 50 m. The wind has very little diurnal variation and is due ''north'' (''up''), as in previous similar figures.

currents can be determined by ensemble averaging the 5-m current over 4-h intervals throughout the day. The inertial period is just under one day at this latitude (34°N), so the diurnal cycle of the current appears much like an inertial oscillation (Fig. 12a). During midafternoon when the mixed layer is shallowest the current reaches its maximum value. The diurnal cycle of the current extends all the way through the upper 50 m, as indicated in the integrated volume transport (Fig. 12b), and further demonstrates how strongly the diurnal thermal cycle affects the wind-driven current.

The diurnal variability in the wind-driven current is relevant to understanding the surface-trapping of the current. Price et al. (1987) demonstrated that modeling the upper ocean as a uniformly accelerated ''slab'' layer whose depth varies throughout the day results in a mean current that is surface-trapped, with a flat spiral, like the observed mean current. Wijffels et al. (1994) also found uniform currents within the mixed layer after removing the geostrophic portion of the current from the total current.

The diurnal progression of the force balance that drives the diurnal cycle in the mean current can be determined if the calculated momentum balance is divided into 4-h intervals throughout the day, then averaged for each interval over the entire record (as we did to determine the diurnal variation of the mean current). The wind stress vector has very little diurnal variation (Fig. 13) and remains almost constant. The force balance (2) is close to being exact throughout the day, despite the very large diurnal variation in the individual terms (except wind stress) as the current rotates through a diurnal oscillation. The horizontal stress divergence ($\partial\tau/\partial z$) has little diurnal variation, which is surprising given the very large diurnal variability of the current. A resolution of this seeming contradiction is to note that 1) diurnal rotation is a nearly free inertial oscillation that does not require a substantial force (horizontal stress divergence) to remain in motion (though the diurnal variation of stratification does serve to help phase lock the rotation to the diurnal cycle) and 2) seasonal stratification was very shallow during July of the LOTUS 3 period (Schudlich 1991) and contributed, along with diurnal variation of stratification, to the strong surface-trapping of the Ekman current.

In contrast to LOTUS 3, there is very little diurnal variability in the LOTUS 4 mean current spiral (Fig. 14). This is consistent with reduced diurnal stratification expected for higher wind stress and reduced insolation during the winter (Bowers et al. 1986). Rather, the structure of the LOTUS 4 mean current spiral is characterized by a persistent downwind shear in the upper 15 m that exhibits almost no diurnal variation. We explore the downwind shear in more detail in the following section.

6. The near-surface downwind shear during LOTUS 4

Aside from the deeper penetration of the mean current and lack of diurnal variability in winter, the major difference between the summer and winter current spirals is the substantial downwind shear in the upper 15 m during winter. This downwind shear above 15 m is evident not only in the mean current (Fig. 6) but throughout the LOTUS 4 record (Fig. 15), despite the fact that the raw currents were usually dominated by mesoscale

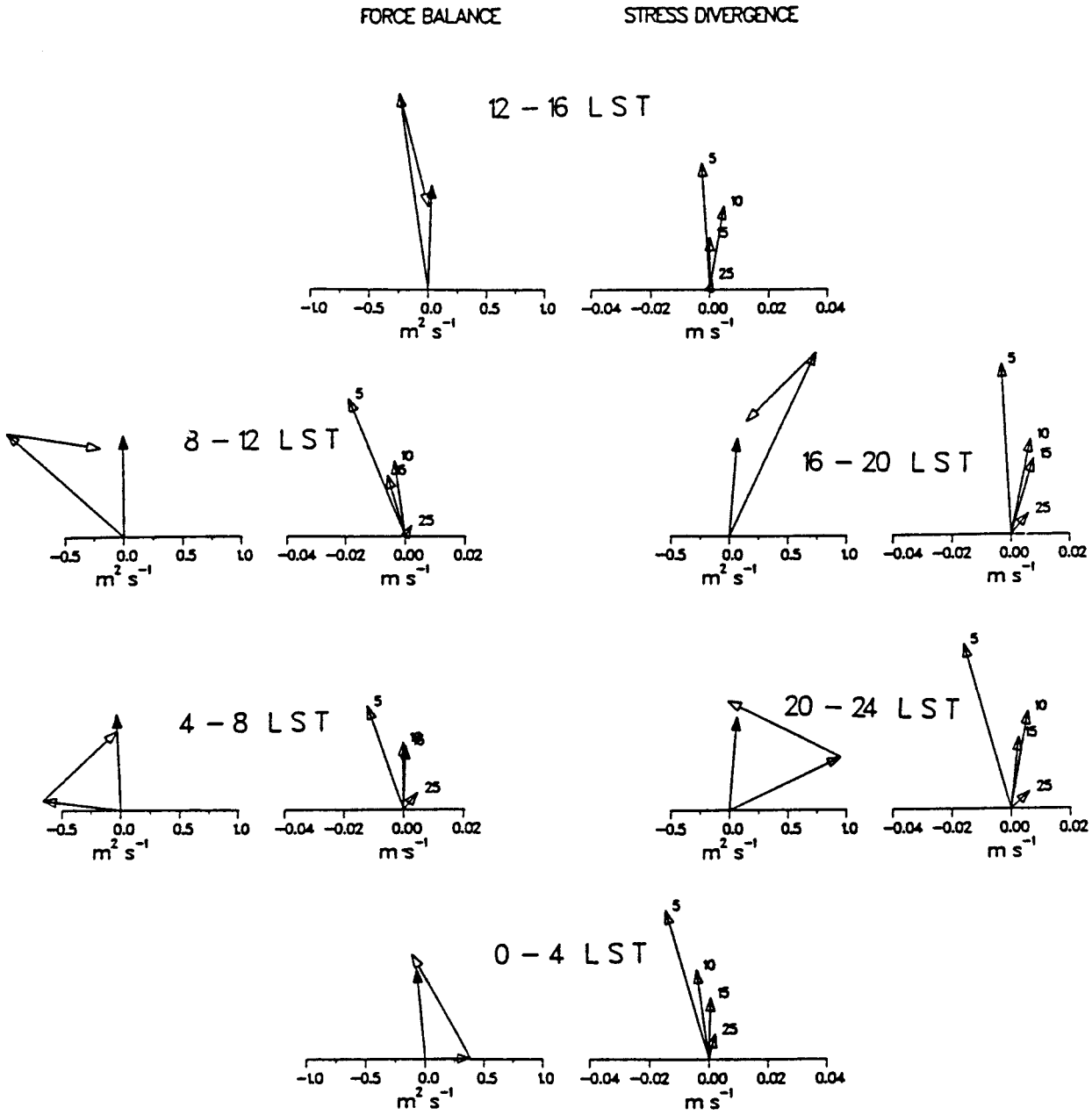

FIG. 13. The diurnal progression of the depth-integrated force balance between the Coriolis force, wind stress, and local acceleration (left-hand side of individual plots) and estimates of the horizontal stress divergence profile, $\partial\tau/\partial z$ (right-hand side of individual plots) during LOTUS 3. The hours (in local solar time, LST) over which the ensemble averages were made are indicated above each pair of plots. The mean wind direction is ''up.'' Numbers at the tips of the $\partial\tau/\partial z$ vectors indicate the depth in meters. In the force balance plots, the wind stress vectors are shown with a solid arrowhead, the Coriolis force vector is shown with an open arrowhead and is plotted with the same origin as the wind stress. The local acceleration vector is also shown with an open arrowhead but is plotted with its tail at the tip of the Coriolis vector, showing how the acceleration turns this vector throughout the 4-h interval.

eddylike motions (Fig. 2). Below 15 m, the shear is much reduced and does not appear to be correlated to the wind. Though the near-surface shear appears strongly correlated with the wind, there were no events that gave any clear indication of the phase relation between changes in the wind and the response of the downwind shear (Schudlich 1991).

The near-surface downwind shear could arise from a variety of sources including a surface-intensified geostrophic flow coupled to the local wind through Ekman pumping, Langmuir circulation, a logarithmic boundary layer, or a surface-wave induced bias. We cannot quantify Ekman pumping with the LOTUS data and can only give generic estimates of the effects of Langmuir cir-

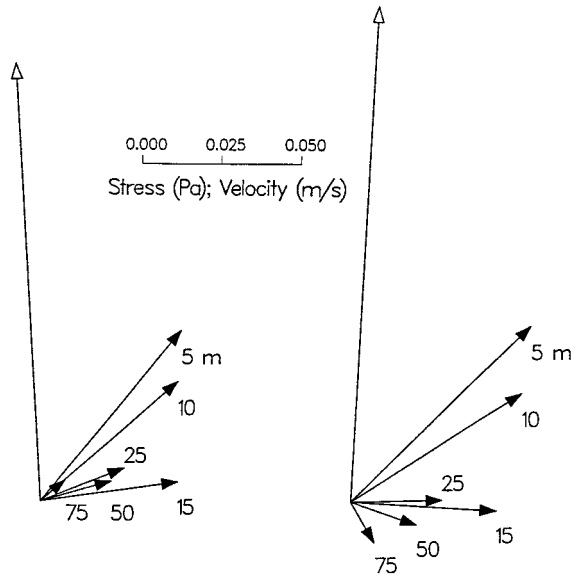

FIG. 14. Diurnal cycle of the LOTUS 4 mean wind stress and mean current spiral (relative to 129 m). The wind stress vector is shown with an open arrowhead, and the numbers at the end of the current vectors indicate the depth in meters. On the left is the mean current during the nighttime hours (2000 to 0800 LST) of the LOTUS 4 data and on the right is the mean current during the daytime hours (0800 to 2000 LST). Note the lack of a diurnal variation in the wind stress, the weak diurnal variation in the currents, and the persistent downwind shear in the upper 15 m.

culations, which we do below. Here we will consider in detail the latter two processes that could produce a downwind shear in the near-surface layer: (i) a logarithmic boundary layer (''wall layer'') and (ii) a surface-wave-induced bias in the measured current. The first process would imply that the momentum balance is not closed within the top 100 m in LOTUS 4, while the second implies that the lack of closure is a measurement problem.

a. Logarithmic boundary layer

The simplest model of the velocity profile near a boundary is the classic ''law of the wall'' (Turner 1973). If stratification is unimportant and if a constant stress layer exists near a solid boundary (or ''wall''), then over distances from the boundary that are small compared to the planetary boundary scale u_*/f, the current will have a logarithmic profile $u(z) = (u_*/\kappa)\ln(z) + c$, where $\kappa = 0.4$ (von Kármán's constant), $u_* = (\tau/\rho)^{1/2}$, and c is a constant of integration. The shear between two levels in a wall layer is then

$$\Delta u = u(z_1) - u(z_2) = (u_*/\kappa)\ln(z_2/z_1) \qquad (3)$$

and is in the direction of the wind stress. Such logarithmic wind profiles are a well-documented phenomenon in the atmospheric boundary layer near the earth's surface (Stull 1988). However, the wall-layer model would seem to oversimplify the ocean surface layer, which is not bounded by a solid surface and is stirred by breaking surface waves and Langmuir circulations. Recent measurements and modeling of turbulent dissipation in the upper ocean suggests that wall-layer shear does not hold under breaking waves within a few wave heights of the surface (Agrawal et al. 1992; Craig and Banner 1994; Anis and Moum 1995). However, some observations of near-surface shear in the ocean are consistent with wall-layer shear (Richman et al. 1987; Lentz 1992). When we calculate the log-layer shear as a function of wind stress, we too find that the downwind shear in LOTUS 4 above 25 m is consistent with both the direction and magnitude of a wall layer shear (Fig. 16); this may be because our shallowest measurement at 5 m is more than ''a few wave heights'' below the surface.

b. Surface-wave-induced bias

Another source of near-surface downwind shear may be the wave-induced motion of a surface buoy, which can be biased into measurements of the current made from a current meter attached to a surface mooring (Pollard 1973). A bias in the direction of the wave phase propagation arises because, as the surface buoy moves vertically and horizontally with the surface waves, the current meters suspended beneath it measure currents in different parts of the water column relative to the mean sea level and relative to a fixed point. The result is that perfect current meters measure a quasi-Eulerian mean current, or ''wave bias,'' even if the Eulerian mean were zero. The kinematics of this wave bias are very similar to that of Stokes drift, and the amplitude is the same at the sea surface. The wave bias decays with depth at half the rate of the comparable Stokes drift since the current meter motion does not decrease with depth. The wave bias is dominated by shorter period wind waves rather than long period swell, and therefore tends to be in the direction of the local wind (Santala 1991).

The wave bias has been estimated at each of the LOTUS current meter depths using a model developed by Santala (1991). This model incorporates the mechanism described by Pollard (1973) into a directional wave spectrum. To accurately estimate the wave bias both the directional wave spectrum and the current meter motion must be known. Unfortunately, neither of these are available from the LOTUS observations. We have therefore estimated the wind wave spectrum from the observed wind speed after Donelan et al. (1985), assuming a wind duration of 12 h estimated from a visual inspection of the wind records and roughly consistent with the 24-h averaging subinterval. We make no correction for swell propagation as this requires detailed wave data that was not available. For the mean wind speed of LOTUS 4 ($u_{\text{wind}} = 10.7$ m s^{-1}) and a wind duration of 12 h, this yields fully developed wind waves ($u_{\text{wind}}/c = 1.0$, where c is the wave phase speed) with a period of 7 s and a significant wave height of 2.4 m (Kitaigorodskii et al. 1983; Kinsman 1965).

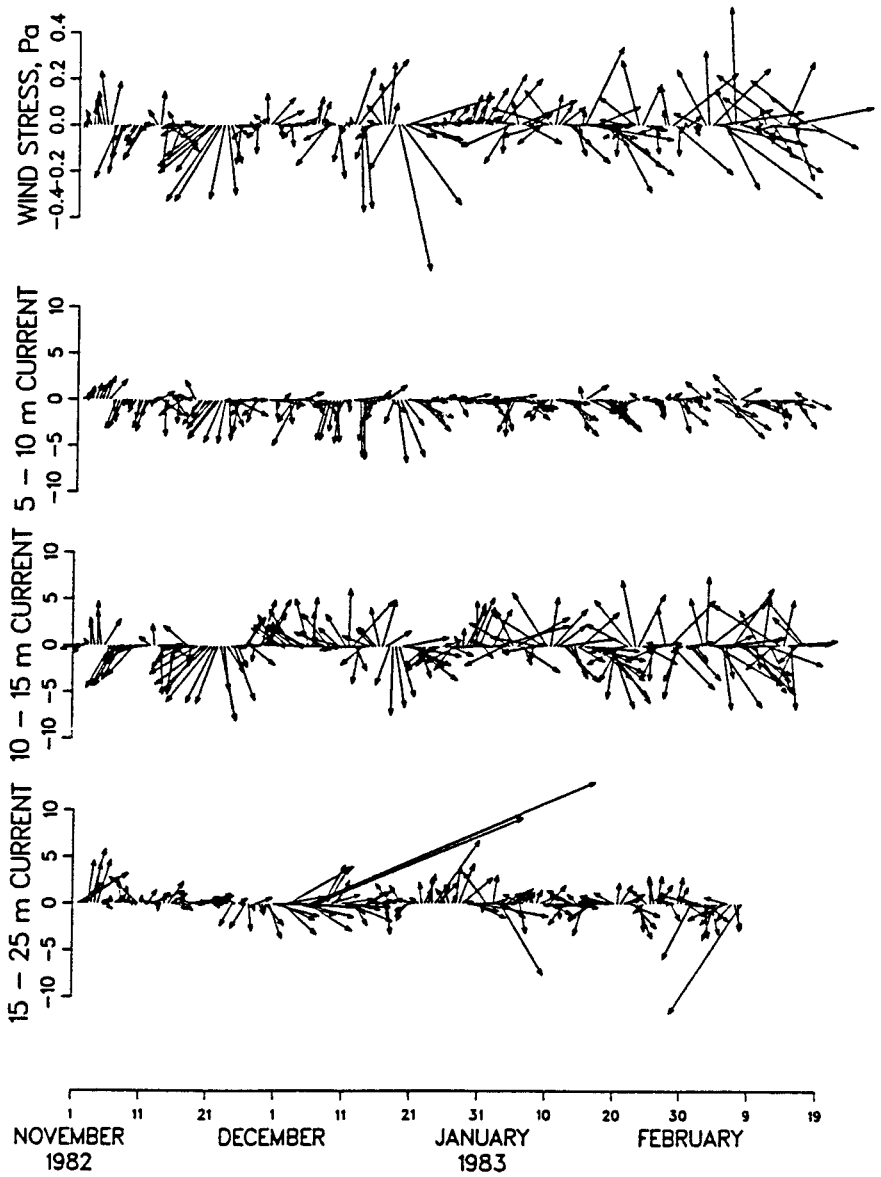

FIG. 15. Wind stress and near-surface shear during LOTUS 4. North is ''up'' and east is to the right. Each vector is a 12-h average. Note the wind-driven signal in the upper 15 m and the larger shear between 10 and 15 m than between 5 and 10 m (the current meter at 15-m depth is a VACM whereas at all other depths currents were measured by VMCMs). The shear in the upper 15 m is strongly correlated with the wind. The two large values in the shear from 15 to 25 m during December are due to data dropout on the VMCM at 25 m, and were not included in the calculation of the mean current. The VMCM at 25 m later failed after 99 days on 9 February.

To estimate the buoy's motion we assume that it is a perfect surface follower, as suggested by Boy (1986) and Berteaux and Boy (1986), for the discus buoys used in the LOTUS experiment. We also assume the instruments move horizontally and vertically in phase with the buoy since the mooring line was very taut (5395 m of mooring line in 5366 m of water). An upper bound on the size of the wave bias is calculated assuming that both vertical and horizontal motion are biased into the measurements, and a lower bound is found by assuming that only vertical motion is biased into the measurements. Berteaux and Boy (1986) indicate that the former is likely to hold, but recent data on tilt–heave buoy motion suggest the latter (A. Gnanadesikan 1995, personal communication).

c. Comparison with observations

Our estimates of the wave bias are the same magnitude as the measured downwind current in the upper

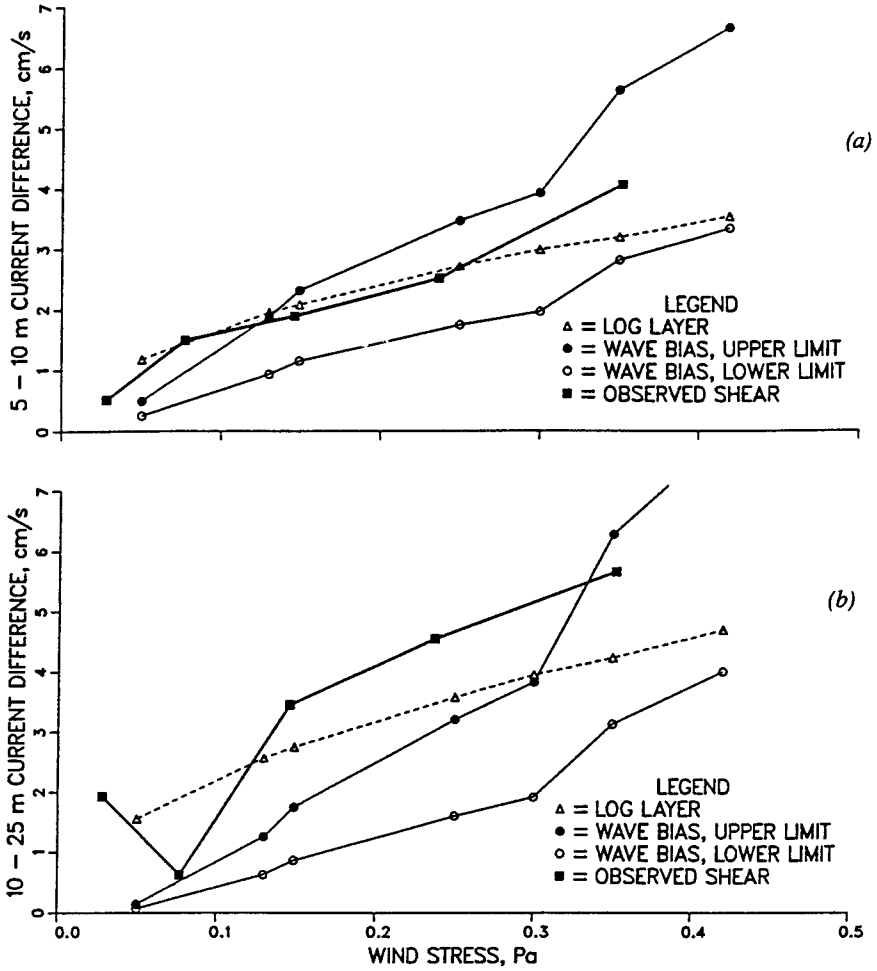

FIG. 16. Near-surface observed shear (a) between 5 and 10 m, (b) between 10 and 25 m, and the shear predicted by the log-layer model and the surface wave bias model as a function of wind stress. Between 5 and 10 m, the shear predicted by the surface wave bias model is approximately the same as that predicted for a log-layer, and both are similar to the observed shear, except at low and high wind stress, where the wave bias is closer to the observed shear. Between 10 and 25 m, the observed shear was larger than both the shear predicted in a log-layer and that predicted by the wave bias model.

15 m (relative to 129 m) during LOTUS 4 (Fig. 17). The downwind shear due to the wave bias is also similar to the observed near-surface downwind shear between 5 and 10 m and grows with increasing wind stress roughly as the observed shear does (Fig. 16a). Thus, the wave bias model gives consistent estimates of the downwind component of the mean current for LOTUS 4 conditions.

However, the shear predicted for a logarithmic boundary layer is also the same magnitude as the observed shear, so the possibility that the observed shear is due to this alternative mechanism cannot be discounted (Fig. 16). The observed shear between 10 and 25 m is greater than both the shear due to the wave bias and the logarithmic boundary layer shear (Fig. 16b), which does not help to resolve the source of the downwind shear.

The most telling difference between these two quite different sources of shear is their dependence upon wind stress amplitude: the log-layer shear is proportional to $u_* \sim \tau^{1/2}$, while the wave bias shear grows roughly like τ at large τ but goes to zero well before τ (Fig. 16). We have sorted the LOTUS 4 observed shear on τ and compare the predictions of the two models of downwind shear. To our eye, the result is sufficiently ambiguous that we cannot reject either one of the models. However, for LOTUS 3 conditions, the predicted log-layer shear is about $1/\sqrt{2} = 0.7$ of the LOTUS 4 shear, or about 3 cm s^{-1} between 25 and 5 m, while the wave bias shear is expected to be about 0.5 cm s^{-1} for the same wind stress (the LOTUS 3 observations show very little excess downwind shear beyond that expected from diurnal cycling; see Figs. 4 and 18). Thus, the wave bias model appears to give a consistent account of downwind shear in both LOTUS 3 and LOTUS 4 conditions, while the log-layer model does not. This result suggests that the

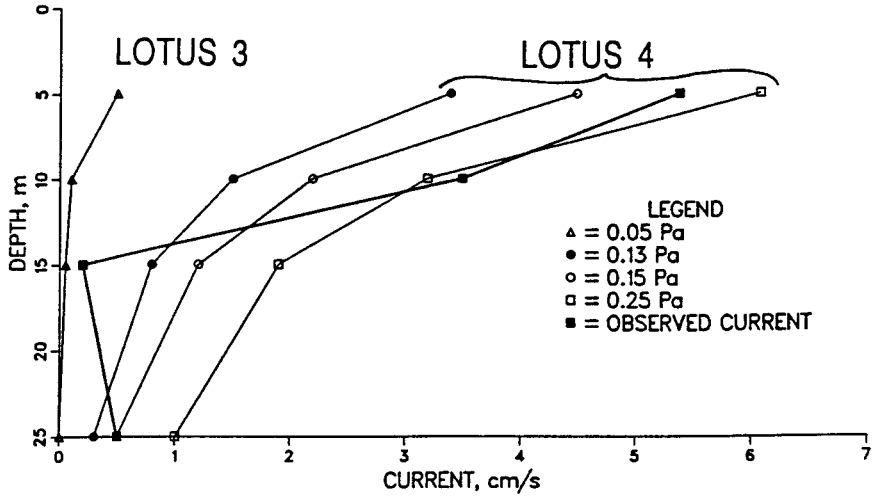

FIG. 17. Profiles of observed mean LOTUS 4 downwind current and the wave bias predicted by the model of Santala (1991) for four different values of wind stress. For LOTUS 4 (winter) conditions, the predicted wave bias is the same order of magnitude as the observed downwind near-surface current. For the lighter winds typical of the LOTUS 3 (summer) conditions, the predicted wave bias is very small. This is consistent with the large mean downwind current observed in the winter (see Fig. 6) and the lack of a mean downwind current in the summer (see Fig. 4). Wave bias estimated from observed directional wave spectra (therefore including swell) from the Acoustic Surface Reverberation Experiment (ASREX) are comparable in magnitude to these results (Gnanadesikan 1994).

downwind shear found in LOTUS 4 is due to wave bias. Langmuir circulations, which cannot be quantified here, could also be a source of this downwind shear. Langmuir cells contain downwind jets that persist at the convergence of the roll cells (Leibovich 1983; Smith et al. 1987; Weller and Price 1988; Li and Garrett 1993; Plueddemann et al. 1996), and thus free-floating or surface-moored instrument platforms may have a sampling bias in this convergence zone. Gnanadesikan and Weller (1995) estimate a Langmuir circulation bias in shear of up to 0.005 s^{-1} at least as deep as 5 m, comparable to the 0.004 s^{-1} of downwind shear between 5 and 10 m the LOTUS 4 mean (Table 1).

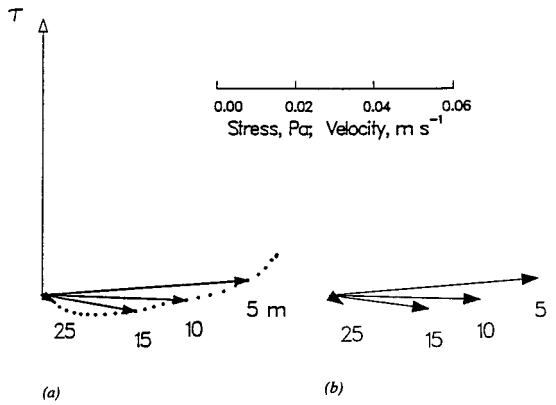

FIG. 18. (a) Numerical simulation of the LOTUS 3 mean current spiral, obtained using the Price et al. (1986) upper-ocean model, and averaged and rotated relative to the wind direction just as was the observed mean spiral shown in Fig. 4. The mean wind stress vector is shown with an open arrowhead; current vectors, shown with solid arrowheads, correspond to the VMCM depths during LOTUS 3 and the dots are at 1-m intervals. The mean simulated transport (not shown) is exactly equal to the Ekman transport. Note that the simulation predicts that the wind-driven current penetrated to *O* (30 m) for the fair, summer conditions of the LOTUS 3 period. (b) Numerical simulation of the LOTUS 3 mean currents, with the ''wave bias'' (estimated using the model of Santala 1991) added to the mean current; discussed in the text in section 6b.

If we calculate a simulation of the LOTUS 3 and 4 periods (using the model of Price et al. 1986) and average it, as we did the observations [as Price et al. (1987) did for LOTUS 3], we can see that the LOTUS 3 simulated spiral is quite similar to the observed spiral (Figs. 4 and 18) while the LOTUS 4 simulation has none of the downwind shear in the upper 25 m that the observed spiral does (Figs. 6 and 19). If the estimated wave bias is then added to the simulated mean currents, it makes little difference in LOTUS 3 (Fig. 18b) since, at 5-m depth, the amplitude of the wave bias estimated for LOTUS 3 conditions is only about 0.5 cm s^{-1} (Fig. 17). However, it makes a substantial difference in the LOTUS 4 case. Comparing Figs. 19b and 6, it is apparent that the combination of the upper ocean and wave bias models gives a spiral quite similar to that observed. The exception is the 15-m current, which, as noted in section 3c, was measured by a VACM rather than by a VMCM. This result strongly suggests that estimates of the wave bias may need to be removed from currents measured from surface moorings in order to obtain the true current near the surface, especially during periods of high winds. Rudnick and Weller (1993) show that currents

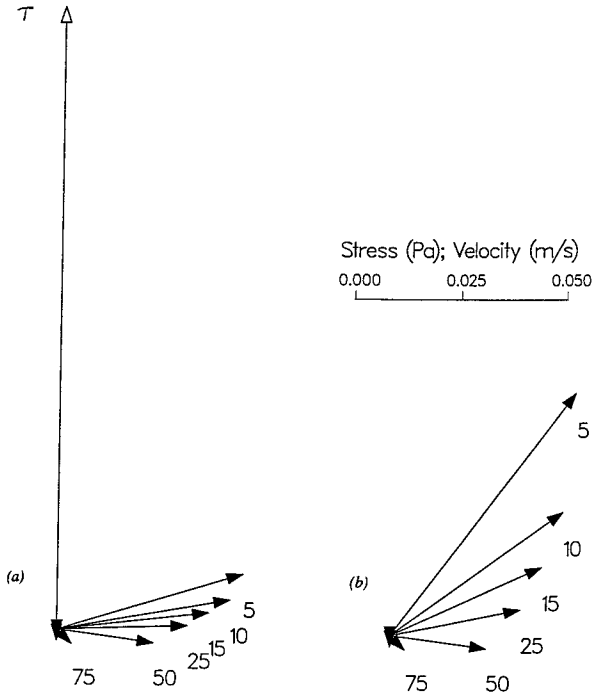

FIG. 19. (a) Numerical simulation of the LOTUS 4 mean current spiral, obtained using the Price et al. (1986) upper-ocean model, and averaged and rotated relative to the wind direction just as was the observed mean spiral, shown in Fig. 6. The mean wind stress vector is shown with an open arrowhead; current vectors, shown with solid arrowheads, correspond to the VMCM depths during LOTUS 4. The mean simulated transport (not shown) is exactly equal to the Ekman transport. Note that the simulation shows no significant downwind shear in the upper 15 m and predicts that the mean wind-driven current penetrated to O (100 m) for the winter conditions prevailing during the LOTUS 4 period. (b) Numerical simulation of the LOTUS 4 mean currents, with the ''wave bias'' (estimated using the model of Santala 1991) added to the mean current, discussed in section 6b.

measured from surface moorings can also be affected by other high-frequency wind-coherent mooring motions, which may be associated with Ekman pumping.

7. Summary and remarks

For both the LOTUS 3 (summer) and LOTUS 4 (winter) deployments the mean current has a spiral structure qualitatively similar to an Ekman spiral, rotating clockwise with depth. The depth scale of the spiral depends on stratification, which was very different in the two seasons. In the summer, net heating and light winds (average wind stress of 0.068 Pa) led to a shallow seasonal stratification and an Ekman layer with an e-folding in 12 m. In the winter, net cooling and strong winds (average wind stress of 0.147 Pa) give an Ekman layer that e-folds in 25 m. In both cases the wind-driven transport is given by the classic Ekman relation to within expected error. To demonstrate this we had to perform wind-relative averaging, which enhanced the wind-driven signal dramatically.

During the summer, the primary variability in the current structure was diurnal, and the mean spiral was relatively ''flat.'' The flatness of the spiral is due to the diurnal cycle in stratification (Price et al. 1987). In the mean, during daytime hours, the Ekman transport is trapped as an intense jet in a shallow surface layer and is essentially to the right of the wind, whereas during evening hours the Ekman jet is spread over a deeper layer that tends to rotate clockwise inertially with time (see Fig. 12b). Instantaneously the Ekman layer is rather slablike, but the average of many such slabs is a mean spiral that, relative to a classic Ekman spiral, decays in magnitude faster than it rotates with depth. Similar results have been found in the upper-ocean studies of Rudnick and Weller (1993), Wijffels et al. (1994), Chereskin (1995), and Lee and Eriksen (1996).

In contrast, the winter current profile had very little diurnal variation (as expected due to stronger winds and reduced diurnal variation in solar heating), and its most striking feature is a persistent downwind shear in the upper 15 m. The downwind shear observed in the winter (LOTUS 4) is consistent both with a logarithmic boundary layer and with the estimated error induced by buoy motion due to surface waves. It is also possible that this downwind shear is at least partially due to a sampling bias caused by Langmuir cells. When we consider the summer (LOTUS 3) conditions, we find that the wave bias model gives a consistent accounting while the log-layer model predicts significant downwind shear where very little occurs. Thus, wave bias and Langmuir circulation bias are the most plausible causes of the downwind shear found in LOTUS 4. Subtracting the estimated wave bias from the observed winter spiral (LOTUS 4), the ''corrected'' winter spiral has a 5-m current amplitude of about 5 cm s^{-1}, much like that of the previous summer (LOTUS 3), and the winter currents at 10 and 15 m are of nearly equal amplitude and 90° to the right of the wind. However, before applying such a correction to field observations, it would be desirable to estimate the surface wave bias from direct observations of the surface waves and the buoy or current meter motion, and to correct for other wind-coherent mooring motions that can contaminate currents measured from surface moorings (Rudnick and Weller 1993).

Acknowledgments. The authors gratefully acknowledge the support of the Office of Naval Research under Grant N00014-89-J-1053 and the National Science Foundation under Award OCE-95-21468. We would also like to thank Markku Santala for the use of his surface wave bias model. Discussions with Susan Wijffels, Harry Bryden, Al Plueddemann, Pierre Mourad, Craig Lee, Meghan Cronin, and Dan Rudnick were very helpful, as were comments on the manuscript from Anand Gnanadesikan and an anonymous reviewer. Nancy Brink's ongoing help with the LOTUS observations has been invaluable.

REFERENCES

Agrawal, Y. C., E. A. Terray, M. A. Donelan, P. A. Hwang, A. J. Williams III, W. M. Drennan, K. K. Kahma, and S. A. Kitaigorodskii, 1992: Enhanced dissipation of kinetic energy beneath surface waves. *Nature,* **359,** 219–220.

Anis, A., and J. N. Moum, 1995: Surface wave–turbulence interactions: Scaling $\varepsilon(z)$ near the sea surface. *J. Phys. Oceanogr.,* **25,** 2025–2045.

Berteaux, H. O., and R. L. Boy, 1986: Wave tank study of moored buoy hulls for air–sea interaction applications. *Proc. of the IEEE Oceans '86 Conf.,* Boston, MA, IEEE, 259–270.

Bevington, P. R., 1969: *Data Reduction and Error Analysis for the Physical Sciences.* McGraw-Hill, 336 pp.

Bowers, C. M., J. F. Price, R. A. Weller, and M. G. Briscoe, 1986: Data tabulations and analysis of diurnal sea surface temperature variability observed at LOTUS. Woods Hole Oceanogr. Inst. Tech. Rep. WHOI-86-5, 51 pp. [Available from Woods Hole Oceanographic Institution, Woods Hole, MA 02543.]

Boy, R. L., 1986: Semi-empirical study of moored buoy hulls for air–sea interaction applications. M.S. thesis, Massachusetts Institute of Technology, 76 pp. [Available from Massachusetts Institute of Technology, Cambridge, MA 02139.]

Briscoe, M. G., and R. A. Weller, 1984: Preliminary results from the Long-Term Upper-Ocean Study (LOTUS). *Dyn. Atmos. Oceans,* **8,** 243–265.

Chereskin, T. K., 1995: Direct evidence for an Ekman balance in the California Current. *J. Geophys. Res.,* **100,** 18 261–18 269.

——, and D. Roemmich, 1991: A comparison of measured and wind-derived Ekman transport at 11°N in the Atlantic Ocean. *J. Phys. Oceanogr.,* **21,** 869–878.

Craig, P. D., and M. L. Banner, 1994. Modeling wave-enhanced turbulence in the ocean surface layer. *J. Phys. Oceanogr.,* **24,** 2546–2559.

Davis, R., R. deSzoeke, D. Halpern, and P. Niiler, 1981: Variability in the upper ocean during MILE. Part 1: The heat and momentum balances. *Deep-Sea Res.,* **28A,** 1427–1451.

Deser, C., R. A. Weller, and M. G. Briscoe, 1983: Long Term Upper Ocean Study (LOTUS) at 34°N, 70°W: Meteorological sensors, data, and heat fluxes for May–October 1982 (LOTUS-3 and LOTUS-4). Woods Hole Oceanogr. Inst. Tech. Rep. WHOI-83-32, 68 pp. [Available from Woods Hole Oceanographic Institution, Woods Hole, MA 02543.]

Donelan, M. A., J. Hamilton, and W. H. Hui, 1985: Directional spectra of wind-generated waves. *Philos. Trans. Roy. Soc. London A,* **315,** 509–562.

Ekman, V. W., 1905: On the influence of the Earth's rotation on ocean currents. *Ark. Mat. Astr. Fys.,* **2,** 1–53.

Gnanadesikan, A., 1994: Dynamics of Langmuir circulations in oceanic surface layers. Ph.D. thesis, MIT/WHOI, 354 pp. [Available from Woods Hole Oceanographic Institution, Woods Hole, MA 02543.]

——, and R. Weller, 1995: Structure and instability of the Ekman spiral in the presence of surface gravity waves. *J. Phys. Oceanogr.,* **25,** 3148–3171.

Huang, N. E., 1979: On surface drift currents in the ocean. *J. Fluid Mech.,* **91,** 191–208.

Kinsman, B., 1965: *Wind Waves: Their Generation and Propagation on the Ocean Surface.* Prentice Hall, 676 pp.

Kitaigorodskii, S. A., M. A. Donelan, J. L. Lumely, and E. A. Terray, 1983: Wave–turbulence interactions in the upper ocean. Part II: Statistical characteristics of wave and turbulent components of the random velocity field in the marine surface layer. *J. Phys. Oceanogr.,* **13,** 1988–1999.

Kraus, W., 1993: Ekman drift in homogeneous water. *J. Geophys. Res.,* **98,** 20 187–20 209.

Large, W. G., and S. Pond, 1981: Open ocean momentum flux measurements in moderate to strong winds. *J. Phys. Oceanogr.,* **11,** 324–336.

Lee, C. M., and C. C. Eriksen, 1996: The subinertial momentum balance of the North Atlantic subtropical convergence zone. *J. Phys. Oceanogr.,* **26,** 1690–1704.

Leibovich, S., 1983: The form and drag of Langmuir circulation. *Ann. Rev. Fluid Mech.,* **15,** 391–427.

Lentz, S. L., 1992: The surface boundary layer in coastal upwelling regions. *J. Phys. Oceanogr.,* **22,** 1517–1539.

Li, M., and C. Garrett, 1993: Cell merging and jet/downwelling ratio in Langmuir circulation. *J. Mar. Res.,* **51,** 737–769.

Lippert, A., and M. G. Briscoe, 1990: Observations and EOF analysis of low-frequency variability in the western part of the Gulf Stream recirculation. *J. Phys. Oceanogr.,* **20,** 646–656.

Plueddemann, A., J. A. Smith, D. M. Farmer, R. A. Weller, W. R. Crawford, R. Pinkel, S. Vagle, and A. Gnanadesikan, 1996: Structure and variability of Langmuir circulation during the Surface Waves Processes Program. *J. Geophys. Res.,* **101,** 3525–3543.

Pollard, R. T., 1973: Interpretation of near-surface current meter observations. *Deep-Sea Res.,* **20,** 261–268.

Price, J. F., R. A. Weller, and R. Pinkel, 1986: Diurnal cycling: Observations and models of the upper ocean response to diurnal heating, cooling, and wind mixing. *J. Geophys. Res.,* **91,** 8411–8427.

——, ——, and R. R. Schudlich, 1987: Wind-driven ocean currents and Ekman transport. *Science,* **238,** 1534–1538.

Richman, J. G., R. A. de Szoeke, and R. E. Davis, 1987: Measurements of near-surface shear in the ocean. *J. Geophys. Res.,* **92,** 2851–2858.

Rudnick, D. L., and R. A. Weller, 1993: Observations of superinertial and near-inertial wind-driven flow. *J. Phys. Oceanogr.,* **23,** 2351–2359.

Santala, M. J., 1991: Surface-referenced current meter measurements. Ph.D. thesis, MIT/WHOI, WHOI 91-35, 276 pp.

Schudlich, R. R., 1991: Upper ocean dynamics during the LOTUS and Tropic Heat experiments. Ph.D. thesis, MIT/WHOI, WHOI 91-29, 158 pp.

Smith, J., R. A. Weller, and R. Pinkel, 1987: Velocity structure in the mixed layer during MILDEX. *J. Phys. Oceanogr.,* **17,** 425–439.

Stramma, L., P. Cornillon, R. A. Weller, J. F. Price, and M. G. Briscoe, 1986: Large diurnal sea surface temperature variability: Satellite and in situ measurements. *J. Phys. Oceanogr.,* **16,** 827–837.

Stull, R. B., 1988: *An Introduction to Boundary Layer Meteorology.* Kluwer Academic, 666 pp.

Tarbell, S. A., N. J. Pennington, and M. G. Briscoe, 1984: A compilation of moored current meter and wind recorder data: Vol. XXXV: Long-Term Upper Ocean Study (LOTUS) (Moorings 764, 765, 766, 767, 770) May 1982–April 1983. Woods Hole Oceanogr. Inst. Tech. Rep. WHOI-84-36, 154 pp. [Available from Woods Hole Oceanographic Institution, Woods Hole, MA 02543.]

Turner, J. S., 1973: *Buoyancy Effects in Fluids.* Cambridge University Press, 368 pp.

Weller, R. A., 1981: Observations of the velocity response to wind forcing in the upper ocean. *J. Geophys. Res.,* **86,** 1969–1977.

——, and R. E. Davis, 1980: A vector measuring current meter. *Deep-Sea Res.,* **27A,** 565–582.

——, and J. F. Price, 1988: Langmuir circulation within the oceanic mixed layer. *Deep-Sea Res.,* **35,** 711–747.

——, and A. J. Plueddemann, 1996: Observations of the vertical structure of the oceanic boundary layer. *J. Geophys. Res.,* **101,** 8789–8806.

——, D. L. Rudnick, C. C. Eriksen, K. L. Polzin, N. S. Oakey, J. W. Toole, R. W. Schmitt, and R. T. Pollard, 1991: Forced ocean response during the Frontal Air–Sea Interaction Experiment. *J. Geophys. Res.,* **96,** 8611–8638.

Wijffels, S., E. Firing, and H. L. Bryden, 1994: Direct observations of the Ekman balance at 10°N in the Pacific. *J. Phys. Oceanogr.,* **24,** 1666–1679.

Worthington, L. V., 1959: The 18° water in the Sargasso Sea. *Deep-Sea Res.,* **5,** 297–305.